PHYSICAL REVIEW B **93**, 180509(R) (2016)

High-pressure magnetic state of MnP probed by means of muon-spin rotation

R. Khasanov,[1,*] A. Amato,[1] P. Bonfà,[2] Z. Guguchia,[1] H. Luetkens,[1] E. Morenzoni,[1] R. De Renzi,[2] and N. D. Zhigadlo[3,4]

[1]*Laboratory for Muon Spin Spectroscopy, Paul Scherrer Institut, 5232 Villigen PSI, Switzerland*

[2]*Dipartimento di Fisica e Scienze della Terra e Unità CNISM di Parma, Università di Parma, 43124 Parma, Italy*

[3]*Laboratory for Solid State Physics, ETH Zurich, 8093 Zurich, Switzerland*

[4]*Department of Chemistry and Biochemistry, University of Bern, 3012 Bern, Switzerland*

(Received 10 March 2016; revised manuscript received 9 May 2016; published 25 May 2016)

We report a detailed muon-spin rotation study of the pressure evolution of the magnetic order in the manganese-based pnictide MnP, which has been recently found to undergo a superconducting transition under pressure once the magnetic ground state is suppressed. Using the muon as a volume sensitive local magnetic probe, we identify a ferromagnetic state as well as two incommensurate helical states (with propagation vectors **Q** aligned along the crystallographic c and b directions, respectively) which transform into each other through first-order phase transitions as a function of pressure and temperature. Our data suggest that the magnetic state from which superconductivity develops at higher pressures is an incommensurate helical phase.

DOI: 10.1103/PhysRevB.93.180509

Recently, the binary pnictides CrAs and MnP have attracted much interest due to the discovery of superconductivity induced by hydrostatic pressure [1–4]. The helical magnet CrAs becomes superconducting for pressures exceeding $p \simeq 0.4$ GPa, whereas MnP possesses a critical pressure $p_c \simeq 8$ GPa at which magnetism disappears and superconductivity sets in. For CrAs, in the pressure range of $0.4 \lesssim p \lesssim 0.7$ GPa, one observes a phase separation between magnetic and paramagnetic volumes, with the latter becoming superconducting with a critical temperature $T_c \lesssim 2$ K. Above 0.7 GPa the helical magnetic order vanishes and superconductivity below T_c sets in within the whole sample volume [5]. Note that in CrAs the single type of helical magnetic order remains unchanged as a function pressure [5]. In comparison to CrAs, MnP possesses a more complicated phase diagram [4]. At ambient pressure, MnP orders ferromagnetically at $T \simeq 290$ K with the Mn magnetic moments aligned along the crystallographic b direction (according to the crystallographic group $Pnma$ 62 with lattice constants $c > a > b$) [6–8]. The ordered moment is $m \simeq 1.29\mu_B$ per Mn atom [6,9]. At lower temperatures ($T \lesssim 50$ K) another transition in a double-spiral helical structure is reported [7,9,10]. In this helimagnetic state (helical-c state [11]) the Mn moments are rotated within the ab plane (helical plane) with the propagation vector $\mathbf{Q} = (0,0,0.117)$ [7]. By increasing pressure the helical phase vanishes at $p \simeq 1$–1.5 GPa and a new magnetic phase emerges for $p \gtrsim 2$ GPa [4]. In a narrow pressure region close to a critical pressure p_c, at which the new magnetic phase disappears, superconductivity is found below 1K. It was suggested that there is a quantum critical point at $p = p_c$ and that the quantum fluctuations persisting above p_c give rise to the occurrence of superconductivity [4]. Therefore, it is important to characterize the high-pressure magnetic state of MnP from which superconductivity emerges. At present, there are three reports based on the results of nonresonant x-ray, NMR, and neutron diffraction experiments pointing to a helical magnetic order [11–13]. Note that the NMR study does not allow one to identify the order, while the nonresonant x-ray and neutron diffraction experiments disagree on the type of high-pressure helix. While the x-ray study points to a similar helical-c structure as the one at ambient pressure, the neutron diffraction study suggests that a conical or two-phase structure with $\mathbf{Q} \parallel b$ develops and it gradually changes to the so-called helical-b structure with Mn moments rotating within the ac plane.

In this Rapid Communication we report on a detailed study of the evolution of magnetic properties of MnP as a function of temperature (5 K $\lesssim T \lesssim$ 300 K) and pressure (0.1 MPa $\leqslant p \lesssim 2.4$ GPa) by means of muon-spin rotation (μSR). The resulting p-T phase diagram [Fig. 1(a)] consists of three areas corresponding to the ferromagnetic (FM), the helical-c (Hel-c), and the helical-b (Hel-b) orders with the corresponding field distributions $P(B)$'s [fast Fourier transform of the zero-field (ZF) μSR data] presented in Figs. 1(b)–1(d), respectively. The phases FM/Hel-c as well as FM/Hel-b are found to coexist within a broad range of pressures and temperatures. Transitions from the high-temperature FM to the low-temperature, low-pressure helical-c, or the low-temperature, high-pressure helical-b phases are of first order. Our experiments confirm that in MnP the high-pressure magnetic phase which is the precursor of the superconducting state is the incommensurate helical-b.

The magnetic response of MnP polycrystalline sample was studied in zero-field (ZF) and weak transverse field (wTF) μSR experiments. A detailed description of μSR experiments under pressure, the construction of the pressure cell, etc., are given in Ref. [14]. In the following we discuss the μSR data for the lowest (0.1 MPa) and the highest (2.42 GPa) pressures.

At ambient pressure, transitions to two different magnetic states are detected [Fig. 2(a)]. The first one at $T_{FM} \simeq 290$ K corresponds to the ferromagnetic order [6,7]. The spontaneous muon-spin precession is clearly observed in the ZF-μSR asymmetry spectra [$A(t)$, Fig. 2(c)]. The oscillatory part of $A(t)$ is well fitted by an exponentially decaying cosine function with a zero initial phase (see the Supplemental Material [15]), thus evidencing that the magnetic order is commensurate [16]. In the low-temperature region, $T \lesssim 25$ K, the oscillatory part of $A(t)$ is accurately described by a field distribution characterized by a minimum (B_{min}) and a maximum (B_{max})

*rustem.khasanov@psi.ch

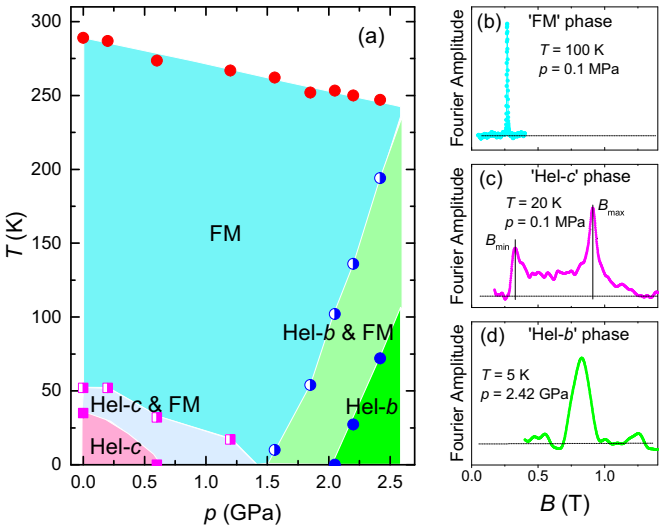

FIG. 1. (a) The p-T phase diagram of MnP obtained from μSR experiments. FM, Hel-c, and Hel-b denote the ferromagnetic, helical-c, and helical-b magnetic orders, respectively (see text). The half solid and solid symbols correspond to the case when the helical-c (pink squares) or the helical-b (blue circles) phases occupy 10% and 90% of the sample volume, respectively. (b)–(d) The magnetic field distribution (fast Fourier transform of the ZF-μSR data) in the FM, Hel-c, and Hel-b state, respectively.

cutoff fields [see Figs. 1(c) and 2(e)], which is consistent with the incommensurate helimagnetic order [17]. In a broad range of temperatures (30 K $\lesssim T \lesssim$ 50 K) both orders are detected simultaneously [Fig. 2(d)]. Being a volume sensitive local probe technique, μSR allows one to follow the temperature evolution of both magnetic phases as demonstrated in Fig. 2(a). The corresponding internal fields in the FM ($B_{\rm int}$) and helical-c ($B_{\rm min}, B_{\rm max}$) phases are presented in Fig. 2(b). The internal magnetic field in the FM phase (i.e., the FM magnetic order parameter) decreases with increasing temperature and vanishes at $T_{\rm FM}$. Analyzing the data with a power law

$$B_{\rm int}(T) = B_{\rm int}(T=0)[1-(T/T_{\rm FM})^{\alpha}]^{\beta} \qquad (1)$$

yields $T_{\rm FM} = 289.0(2)$ K, $B_{\rm int}(T=0) = 0.2925(2)$ T, $\alpha = 1.16(1)$, and $\beta = 0.252(3)$. The value of β lies quite close to the critical exponent $\beta \simeq 1/3$ expected for a second-order phase transition in a three-dimensional (3D) magnetic system [18]. In contrast, both $B_{\rm min}$ and $B_{\rm max}$, which are measures of the magnetic order parameter of the helical-c state, abruptly drop to zero at the phase transition [Fig. 2(b)]. This, together with the coexistence of the FM and helical-c phases in a relatively large temperature region of $\sim$ 20 K, indicates the first-order character of the transition.

At $p = 2.42$ GPa, the transition into the FM state is clearly detected via the observation of a spontaneous muon-spin precession frequency for temperatures below 250 K. Upon decreasing the temperature, another phase, with an internal field approximately 2.5 times higher, starts to develop for $T \lesssim 200$ K and occupies the full sample volume for $T \lesssim 50$ K [Figs. 3(a) and 3(b)]. This phase corresponds to the "unknown antiferromagnetic" phase which was first reported in Ref. [4]. A preliminary analysis reveals that the oscillatory part of the μSR signal in the low-temperature phase is well fitted by the Gaussian decaying cosine function with zero initial phase. The temperature dependences of the magnetic volume fractions and the internal fields obtained for the FM and the low-temperature magnetic phases are shown in Figs. 3(a) and

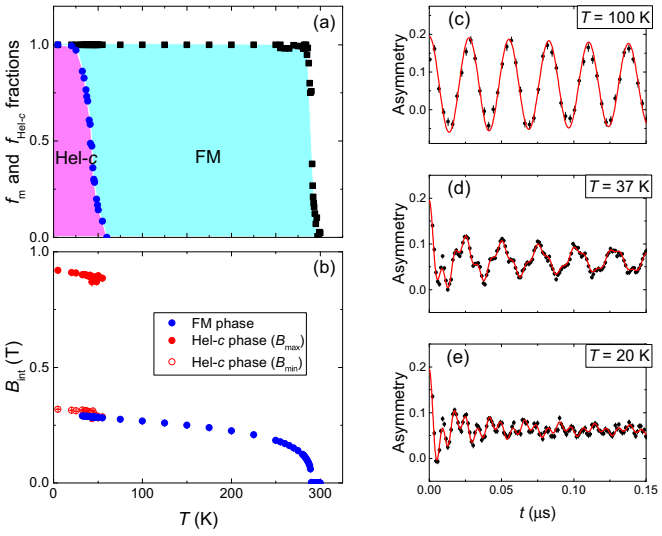

FIG. 2. The magnetic response of MnP at ambient pressure (0.1 MPa). (a) Temperature evolution of the total magnetic volume fraction ($f_{\rm m}$, black squares) and the helical-c fraction ($f_{\rm Hel}$, blue circles). (b) Temperature dependence of internal fields within the FM and helical-c phases. (c)–(e) ZF-μSR asymmetry spectra at $T = 100$ K (FM phase), $T = 37$ K (mixture of FM and helical-c phases), and $T = 20$ K (helical-c phase). Solid red lines are fits as described in the Supplemental Material Ref. [15].

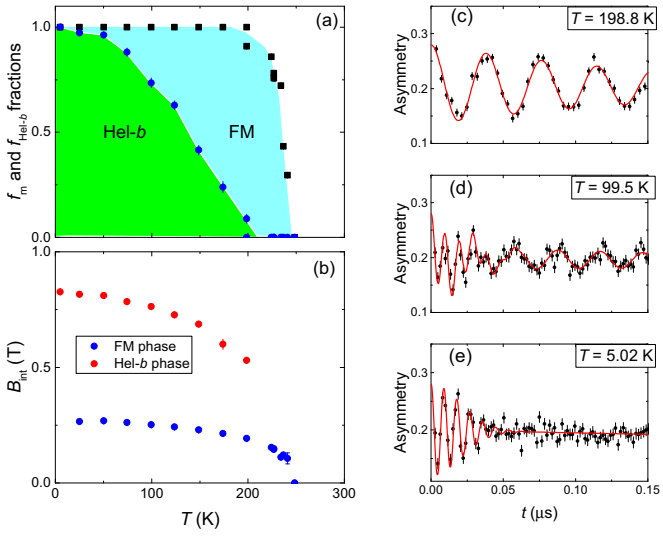

FIG. 3. Magnetic response of MnP at $p = 2.42$ GPa. (a) Temperature evolution of the total magnetic volume fraction ($f_{\rm m}$, black squares) and the high-pressure (helical-b) fraction ($f_{\text{Hel-}b}$, blue circles). (b) Temperature dependence of internal fields within the FM and helical-b phases. (c)–(e) ZF-μSR asymmetry spectra at $T = 198.8$ K (FM phase), $T = 99.5$ K (mixture of FM and helical-b phases), and $T = 5.02$ K (helical-b phase). Solid red lines are fits as described in the Supplemental Material Ref. [15].

3(b). The asymmetry spectra taken at $T \simeq 200$ K (FM phase), $\simeq 100$ K (mixture of FM and magnetic phases), and $\simeq 5$ K (high-pressure magnetic phase), are shown in Figs. 3(c)–3(e), respectively.

At first glance the ambient pressure and $p = 2.42$ GPa data presented in Figs. 2 and 3 look similar. Indeed, (i) in both cases the ferromagnetic phase observed at high temperatures is fully replaced by a low-temperature phase. (ii) Within a broad range of temperatures the ferromagnetic and low-temperature phases coexist. (iii) The appearance of the low-temperature phase is always associated with an abrupt change of the internal field (magnetic order parameter), i.e., there is a first-order transition between the FM and both low-temperature phases.

There is, however, an important difference between them. At ambient pressure the Mn moments form the so-called "double-helical" structure with the propagation vector $\mathbf{Q} = (0,0,0.117)$. Considering four Mn atoms per unit cell, the term "double helical" means that the Mn spins are coupled in pairs (Mn1/Mn4 and Mn2/Mn3), and rotate with a constant phase difference between the different pairs along $\mathbf{Q}$ (see Ref. [7]). Such an incommensurate magnetic structure leads to a field distribution given by [17]

$$P(B) = \frac{2}{\pi} \frac{B}{\sqrt{\left(B^2 - B_{\text{min}}^2\right)\left(B_{\text{max}}^2 - B^2\right)}} \qquad (2)$$

and is characterized by two peaks at a minimum (B_{min}) and a maximum (B_{max}) cutoff field [Fig. 1(c)].

The magnetic field distribution in the high-pressure phase is, however, different. It is characterized by a *single* symmetric line [Fig. 1(d)], though with a very broad width. At first glance such $P(B)$ is inconsistent with the helical order. However, as shown below, the unique situation realized in MnP may lead to the formation of a quasisingle peak structure. In short, in MnP muons stop at four well-defined interstitial lattice sites within the unit cell. The μSR asymmetry spectra consist, therefore, of four contributions, with each of them characterized by its own B_{min} and B_{max} fields and corresponding $P(B)$'s described by Eq. (2). Under certain conditions which, as shown in the Supplemental Material Ref. [15], are fulfilled in MnP for a helical-b magnetic order, the sum of the four asymmetric $P(B)$ distributions results in a single broad symmetric line.

The exact spin arrangement of the high-pressure magnetic phase is currently under debate. It is also not clear whether this phase has a nonzero net magnetic moment. Following Fig. S2 in the Supplemental Material of Ref. [4], the ferromagnetic component of the high-pressure phase might be quite substantial and correspond to $\sim 5\% - 20\%$ of that in the FM phase. The authors of Ref. [11] have also suggested a conical magnetic structure for $p \gtrsim 1.5$ GPa with a ferromagnetic component gradually decreasing with decreasing temperature and increasing pressure. We checked for a possible ferromagnetic component by studying the pressure cell response in wTF μSR experiments. Note that the spins of the muons stopping in the pressure cell containing the magnetic sample will undergo a precession around the vector sum of the weak externally applied field and the stray fields induced by the sample. If these stray fields are sizable and inhomogeneous, as expected around a ferromagnetic sample,

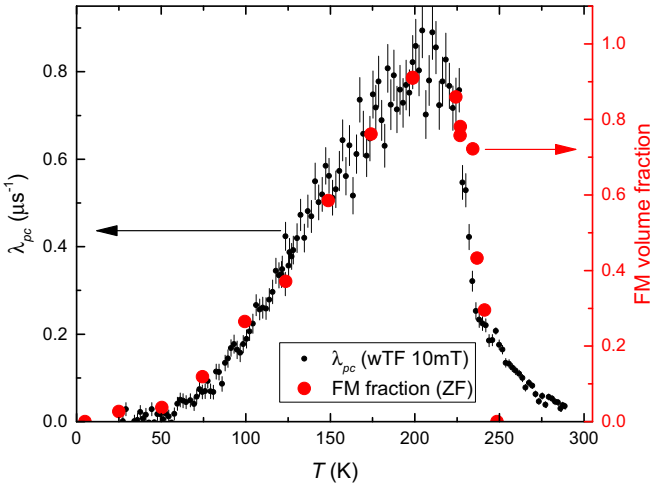

FIG. 4. Temperature dependences of λ_{pc} obtained in 10 mT wTF μSR experiments (black dots) and the FM volume fraction f_{FM} measured in ZF-μSR experiments (red circles) at $p = 2.42$ GPa.

the μSR signal of the muons stopping in the cell will exhibit a relaxation due to dephasing [19].

Figure 4 shows the temperature dependence of an additional exponential relaxation of the spin polarization for the muons stopping in the pressure cell (λ_{pc}). The magnetic field $\mu_0 H = 10$ mT, transverse to the initial muon-spin polarization, was applied at $T \simeq 300$ K (above the magnetic transition). For comparison we also plot in this graph the temperature evolution of the ferromagnetic volume fraction ($f_{\text{FM}} = f_{\text{m}} - f_{\text{hel-}b}$) as obtained in ZF-$\mu$SR experiments [Fig. 3(a)]. Below $T \simeq 250$ K, λ_{pc} follows *exactly* f_{FM}. With decreasing temperature both quantities first increase, thus showing the formation of the FM phase. Both λ_{pc} and f_{FM} saturate at $T \simeq 200$ K, and then decrease almost linearly with temperature decrease from $\simeq 200$ K down to $\simeq 50$ K. Below 50 K, where the FM phase completely vanishes, the signal of the pressure cell becomes unaffected by the sample. This proves that the magnetic order induced by high pressure in the MnP sample possesses no sizable ferromagnetic component and allows one to exclude the conical magnetic structure from consideration.

Additional experiments performed in the intermediate range of pressures ($p = 0.2$, 0.6, 1.2, 1.56, 1.8, 2.05, and 2.20 GPa) allow us to construct the full p-T phase diagram as shown in Fig. 1(a). It resembles the one reported in Ref. [4], with, however, some important differences. First, the transition temperature of the FM state changes quite monotonically with pressure without a pronounced dT_c/dp slope change at $p \sim 2$ GPa. The slope $dT_c/dp = -17.5(9)$ K/GPa is in agreement with the results of Banus [20], reporting $dT_c/dp = -18.5$ K/GPa for pressures ranging $0 \leqslant p \lesssim 2.0$ GPa. Second, there is a broad temperature range where FM and helical-c (at low temperatures and low pressures), and FM and helical-b (at low temperatures and high pressures) orders coexist. We do not detect, however, any coexistence of helical-c and helical-b magnetic orders.

All of above conclusions do not require any particular modeling and are obvious already from the μSR raw data. To obtain more quantitative information, calculations of local

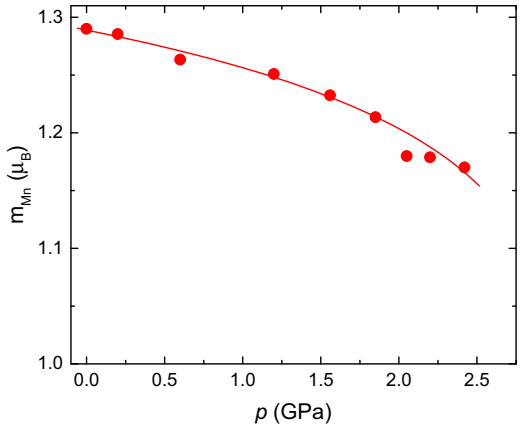

FIG. 5. Pressure dependence of the ordered moment m in the FM state. The line is the guide for the eye.

fields ($B_{\rm loc}$) at the muon stopping sites were carried out. The muon site was determined based on the density-functional theory (DFT) approach, which was shown to accurately determine the muon sites in different materials as, e.g., wide-gap semiconductors, insulating systems, or cuprate- and iron-based high-T_c superconductors [21–26]. There are four equivalent minima in the unit cell corresponding to the 4c [$(x,1/4,z)$,$x_\mu = 0.103$,$z_\mu = 0.921$] Wyckoff position (see the Supplemental Material Ref. [15]). The calculations were started from the known FM and helical-c magnetic structures at ambient pressure (see Refs. [6,7,9,10]). From this first step one could determine the coupling contact constant $A_{\rm cont} \simeq -0.447$ T/$\mu_{\rm B}$ [27]. As a next step, by assuming $A_{\rm cont}$ and the relative positions of Mn ions and muons within the unit cell are pressure independent, as well as accounting for the pressure reduction of lattice constants [12], the pressure dependence of the ordered moment m in the FM state was calculated (Fig. 5). The internal field at $T = 0$ was obtained from the fit of $B_{\rm int}(T)$ by means of Eq. (1) measured at each particular pressure. We have also checked for consistency of the high-pressure magnetic phase with three possible collinear antiferromagnetic structures reported in Ref. [28] and the helical structure proposed in Ref. [12]. The analysis reveals that none of them are consistent with the experimental data (see the Supplemental Material Ref. [15]).

To test whether the helical-b structure proposed in Ref. [11] is compatible with our data, we started first by calculating the $B_{\rm min}$ and $B_{\rm max}$ fields for each particular muon site in the range of $-0.14 \leqslant \delta \leqslant 0.14$ and $-0.16 \leqslant e \leqslant 0.16$. Here, δ is the component of the propagation vector $\mathbf{Q} = (0,\delta,0)$ (the positive and the negative sign correspond to a right- and a left-handed helix, respectively) and $e = (m_a - m_c)/(m_a + m_c)$ is the eccentricity of the elliptical helical-b structure (m_a and m_c are components of m along the a and c axis, respectively). With such determined sets of $B_{\rm min}$'s and $B_{\rm max}$'s the experimental asymmetry spectra were fitted. The correlation plots $\chi^2(\delta,e)$ and $m(\delta,e)$ allow us to check for the range of consistency of helical-b structure with the experimental data and to obtain the value of the average moment m. With $\delta = \pm 0.09$ [11], e and m were found to range $-0.025 \lesssim e \lesssim 0.05$ and $1.175\mu_{\rm B} \lesssim m \lesssim 1.190\mu_{\rm B}$, respectively. Note that the value of m in the helical-b state is close to that determined in the ferromagnetic state $m_{\rm FM} = 1.17\mu_{\rm B}$. The details of calculations are summarized in the Supplemental Material Ref. [15].

To conclude, the muon-spin rotation measurements of MnP under the pressure up to $\simeq 2.4$ GPa were carried out. The ferromagnetic ordering temperature and the value of the ordered Mn moments decrease with the pressure increase from $T_{\rm FM} = 289.0(2)$ K and $m = 1.29\mu_{\rm B}$ at $p = 0.1$ MPa, to $T_{\rm FM} = 242.0(2.2)$ K and $m = 1.17\mu_{\rm B}$ at $p = 2.42$ GPa, respectively. For pressures in the region 0.1 MPa $\leqslant p \lesssim 1.2$ GPa, the ferromagnetic and the helical-c types of magnetic order were clearly detected. The helical-c order becomes completely suppressed for pressures exceeding 1.5 GPa. Above this pressure the third magnetic phase, the helical-b phase [11], starts to grow. The transition temperature and the volume fraction of the helical-b phase increase continuously with increasing pressure. At $p = 2.42$ GPa the helical-b phase was clearly detected up to $T \simeq 200$ K. Pairs of phases, FM/Hel-c and FM/Hel-b, coexist within a broad range of pressures and temperatures. Transitions from the high-temperature FM to the low-pressure helical-c, or the high-pressure helical-b phases, are first-order like.

Note added. Recent DFT calculations have confirmed the nature of heilical-b type of magnetic structure at high pressures [29]. The review on muon-site calculations and on influence of muons on closed surroundings are given at [30].

ACKNOWLEDGMENTS

The work was fully performed at the Swiss Muon Source (SμS), PSI, Villigen. The work of Z.G. was supported by the Swiss National Science Foundation (Switzerland) (Grant No. 200021-149486). P.B. thanks the computing resources provided by CINECA within the Scientific Computational Project CINECA, HP10C5EHG5, 2015, and and STFC's Scientific Computing Department. The work P.B.and R.D.R. was supported by the grants from MUON JRA of FP7 (Belgium), 226507. R.D.R. acknowledges financial support provided by the European Union Horizon 2020 research and innovation programme under Grant Agreement No. 654000.

[1] W. Wu, J. Cheng, K. Matsubayashi, P. Kong, F. Lin, C. Jin, N. Wang, Y. Uwatoko, and J. Luo, Nat. Commun. **5**, 5508 (2014).

[2] H. Kotegawa, S. Nakahara, H. Tou, and H. Sugawara, J. Phys. Soc. Jpn. **83**, 093702 (2014).

[3] H. Kotegawa, S. Nakahara, R. Akamatsu, H. Tou, H. Sugawara, and H. Harima, Phys. Rev. Lett. **114**, 117002 (2015).

[4] J.-G. Cheng, K. Matsubayashi, W. Wu, J. P. Sun, F. K. Lin, J. L. Luo, and Y. Uwatoko, Phys. Rev. Lett. **114**, 117001 (2015).

[5] R. Khasanov, Z. Guguchia, I. Eremin, H. Luetkens, A. Amato, P. K. Biswas, C. Rüegg, M. A. Susner, A. S. Sefat, N. D. Zhigadlo, and E. Morenzoni, Sci. Rep. **5**, 13788 (2015).

[6] E. E. Huber and D. H. Ridgley, Phys. Rev. **135**, A1033 (1964).
[7] G. Felcher, J. Appl. Phys. **37**, 1056 (1966).
[8] T. Yamazaki, Y. Tabata, T. Waki, T. J Sato, M. Matsuura, K. Ohoyama, M. Yokoyama, and H. Nakamura, J. Phys. Soc. Jpn. **83**, 054711 (2014).
[9] H. Obara, Y. Endoh, Y. Ishikawa, and T. Komatsubara, J. Phys. Soc. Jpn. **49**, 928 (1980).
[10] J. Forsyth, S. Pickart, and P. Brown, Proc. Phys. Soc. **88**, 333 (1966).
[11] M. Matsuda, F. Ye, S. E. Dissanayake, J.-G. Cheng, S. Chi, J. Ma, H. D. Zhou, J.-Q. Yan, S. Kasamatsu, O. Sugino, T. Kato, K. Matsubayashi, T. Okada, and Y. Uwatoko, Phys. Rev. B **93**, 100405(R) (2016).
[12] Y. Wang, Y. Feng, J.-G. Cheng, W. Wu, J. L. Luo, and T. F. Rosenbaum, arXiv:1511.09152.
[13] G. Z. Fan, B. Zhao, W. Wu, P. Zheng, and J. L. Luo, Sci. China-Phys. Mech. Astron. **59**, 657403 (2016).
[14] R. Khasanov, Z. Guguchia, A. Maisuradze, D. Andreica, M. Elender, A. Raselli, Z. Shermadini, T. Goko, F. Knecht, E. Morenzoni, and A. Amato, High Pressure Research **36**, 140 (2016).
[15] See Supplemental Material at http://link.aps.org/supplemental/10.1103/PhysRevB.93.180509 for brief information on the sample preparation and data analysis procedure as well on calculations of the muon stopping sites and internal fields on muon positions.
[16] A. Yaouanc and P. Dalmas de Réotier, *Muon Spin Rotation, Relaxation and Resonance: Applications to Condensed Matter* (Oxford University Press, Oxford, UK, 2011).
[17] A. Schenck, D. Andreica, F. N. Gygax, and H. R. Ott, Phys. Rev. B **65**, 024444 (2001).
[18] L. J. De Jongh and A. R. Miedema, Adv. Phys. **23**, 1 (1974).
[19] A. Maisuradze, A. Shengelaya, A. Amato, E. Pomjakushina, and H. Keller, Phys. Rev. B **84**, 184523 (2011).
[20] M. D. Banus, J. Solid State Chem. **4**, 391 (1972).
[21] F. Bernardini, P. Bonfa, S. Massidda, and R. De Renzi, Phys. Rev. B **87**, 115148 (2013).
[22] J. S. Möller, D. Ceresoli, T. Lancaster, N. Marzari, and S. J. Blundell, Phys. Rev. B **87**, 121108(R) (2013).
[23] S. J. Blundell, J. S. Möller, T. Lancaster, P. J. Baker, F. L. Pratt, G. Seber, and P. M. Lahti, Phys. Rev. B **88**, 064423 (2013).
[24] J. S. Möller, P. Bonfa, D. Ceresoli, F. Bernardini, S. J. Blundell, T. Lancaster, R. De Renzi, N. Marzari, I. Watanabe, S. Sulaiman, and M. I. Mohamed-Ibrahim, Phys. Scr. **88**, 068510 (2013).
[25] A. Amato, P. Dalmas de Réotier, D. Andreica, A. Yaouanc, A. Suter, G. Lapertot, I. M. Pop, E. Morenzoni, P. Bonfà, F. Bernardini, and R. De Renzi, Phys. Rev. B **89**, 184425 (2014).
[26] N. Martin, M. Deutsch, F. Bert, D. Andreica, A. Amato, P. Bonfà, R. De Renzi, U. K. Rößler, P. Bonville, L. N. Fomicheva, A. V. Tsvyashchenko, and I. Mirebeau, Phys. Rev. B **93**, 174405 (2016).
[27] In Mn containing binary compounds, such as MnSi [25] and MnGe [26], the contact contribution to the total field is found to be about twice as large as the dipolar one and it has opposite sign.
[28] Z. Gercsi and K. G. Sandeman, Phys. Rev. B **81**, 224426 (2010).
[29] P. Bonfa, I. J. Onuorah, and R. De Renzi, arXiv:1603.08891.
[30] P. Bonfà and R. De Renzi, arXiv:1604.03281.